THE JOURNAL OF BIOLOGICAL CHEMISTRY VOL. 282, NO. 1, pp. 667–679, January 5, 2007

Structural Basis for the Interaction of the Myosin Light Chain Mlc1p with the Myosin V Myo2p IQ Motifs*[S]

Received for publication, July 24, 2006, and in revised form, October 25, 2006 Published, JBC Papers in Press, October 29, 2006, DOI 10.1074/jbc.M607016200

Matteo Pennestri[‡], Sonia Melino[‡], Gian Marco Contessa[‡], Elena Caroli Casavola[§1], Maurizio Paci[‡], Antonella Ragnini-Wilson[§], and Daniel O. Cicero[‡2]

From the Departments of [‡]Chemical Science and Technology and [§]Biology, Università di Roma "Tor Vergata," Via della Ricerca Scientifica 1, 00133 Rome, Italy

Calmodulin, regulatory, and essential myosin light chain are evolutionary conserved proteins that, by binding to IQ motifs of target proteins, regulate essential intracellular processes among which are efficiency of secretory vesicles release at synapsis, intracellular signaling, and regulation of cell division. The yeast *Saccharomyces cerevisiae* calmodulin Cmd1 and the essential myosin light chain Mlc1p share the ability to interact with the class V myosin Myo2p and Myo4 and the class II myosin Myo1p. These myosins are required for vesicle, organelle, and mRNA transport, spindle orientation, and cytokinesis. We have used the budding yeast model system to study how calmodulin and essential myosin light chain selectively regulate class V myosin function. NMR structural analysis of uncomplexed Mlc1p and interaction studies with the first three IQ motifs of Myo2p show that the structural similarities between Mlc1p and the other members of the EF-hand superfamily of calmodulin-like proteins are mainly restricted to the C-lobe of these proteins. The N-lobe of Mlc1p presents a significantly compact and stable structure that is maintained both in the free and complexed states. The Mlc1p N-lobe interacts with the IQ motif in a manner that is regulated both by the IQ motifs sequence as well as by light chain structural features. These characteristic allows a distinctive interaction of Mlc1p with the first IQ motif of Myo2p when compared with calmodulin. This finding gives us a novel view of how calmodulin and essential light chain, through a differential binding to IQ1 of class V myosin motor, regulate this activity during vegetative growth and cytokinesis.

Myosin V are processive motors that transport a variety of intracellular cargo in a manner that is timely, selectively, and reversibly regulated by its interaction with different proteins via their cargo bound domain (1, 2). Myosin V display a dimeric heavy chain containing several light chain binding sites called IQ motifs. The so-called IQ motif (~23–25 residues), with a consensus sequence of the form IQ*XXX*RG*XXX*R, is repeated tandemly (2–6 times) in the heavy chain of many myosins. These motifs are among the best known Ca^{2+}-independent calmodulin (CaM)[3] and myosin light chain targets. Single or multiple repeats IQ motif-like sequences have been identified in myosin, kinases, and IQGAP-like and Ras-GEF signaling proteins in Alzheimer disease proteins (3–5). Tissue myosin V copurify with at least two light chains in addition to calmodulin, but the identity and binding sites of these light chains are unknown (6). It has been shown that either an essential light chain or CaM can occupy the first IQ motif of myosin V (7, 8). How such differential interaction is achieved is unknown. Nor is it clear if and when essential light chain and CaM compete for the same site (4, 9–11). Recent structural and genetic studies point to a previously uncovered role for calmodulin/myosin light chain interaction with the class V myosin IQ motifs in regulating the cargo binding abilities of this class of motors (12–14) in addition to regulate its myosin V processivity (4, 9).

Yeast calmodulin (Cmd1) was the first myosin light chain discovered in *Saccharomyces cerevisiae*, (9). Among the Cmd1 targets there is the class V myosin Myo2p to which the essential myosin light chain 1 (Mlc1p) also binds (15). Unlike calmodulin, Mlc1p does not bind to calcium or other divalent ions (3, 10). Mlc1p interaction with Myo2p IQ motifs is essential for yeast cell viability being required for the polarized delivery of secretory vesicles to the mother-bud neck during cytokinesis (15, 16). This interaction is stimulated by the activation of a Rab/Ypt small GTPase Ypt32p that is involved in vesicle transport (17).

One of the puzzling features of the mechanism by which CaM and myosin light chain by binding to IQ motifs regulate target protein activity is given by the redundancy of IQ motifs in myosins as well as by the presence in the cellular environment of several types of light chain and target IQ motifs. How each light chain specifically recognizes its target IQ motif and by which mechanism such an interaction regulates target protein activity is unclear. The flexibility of light chain structure as well as that of the target protein upon CaM or light chain interaction

* This work was supported in part by the Telethon Foundation-Italy and by funds of the Ministero dell'Istruzione dell'Università e della Ricerca (PRIN programs) and FIRB (programs for basic research). The costs of publication of this article were defrayed in part by the payment of page charges. This article must therefore be hereby marked "*advertisement*" in accordance with 18 U.S.C. Section 1734 solely to indicate this fact.

[S] The on-line version of this article (available at http://www.jbc.org) contains supplemental data.

The atomic coordinates and structure factors (code 2FCD and 2FCE) have been deposited in the Protein Data Bank, Research Collaboratory for Structural Bioinformatics, Rutgers University, New Brunswick, NJ (http://www.rcsb.org/).

[1] Supported by a Telethon Ph.D. fellowship from Grant GGP030341.

[2] To whom correspondence should be addressed: Dept. of Chemical Science and Technology, Università di Roma "Tor Vergata" Via della Ricerca Scientifica 1, 00133 Rome, Italy. Tel.: 39-06-72594835; Fax: 39-06-72594328; E-mail: cicero@scienze.uniroma2.it.

[3] The abbreviations used are: CaM, calmodulin; HSQC, heteronuclear single quantum correlation; RDC, Residual dipolar coupling; SVD, singular value decomposition; r.m.s.d., root mean square deviation; NOESY, two-dimensional nuclear Overhauser effect (NOE) spectroscopy; RLC, regulatory light chain; ELC, essential light chain .

with IQ motifs might be one of the mechanisms by which such regulation is achieved (10, 14, 16, 18).

No structure is available for the isolated Mlc1p protein either in the crystalline state or in solution. The structure of complexes of Mlc1p with three of the six Myo2p IQ motifs were solved by x-ray crystallography (10, 18). Like all other members of the calmodulin superfamily, the structure of Mlc1p shows a dumbbell-shaped structure with similar N- and C-terminal lobes, each of which contains two EF-hand motifs flanked by tightly structured domains. Depending on the IQ sequence, Mlc1p is capable of binding Myo2p using both lobes (IQ2 and IQ3) or only the C-lobe (IQ4). When it interacts with the IQ motif, the N-lobe displays a closed conformation, whereas the C-lobe undergoes upon binding a conformational change, leading to a semi-open conformation (19).

To understand how calmodulin and Mlc1p differently and/or co-ordinately regulate Myo2p activity during cytokinesis by responding to different intracellular signals, we have used NMR analysis to determine the structure assumed by Mlc1p before Myo2p IQ motif binding. In addition, we have mapped the region of Mlc1p involved in the interaction with the first three IQ motifs present in Myo2p. Our results show that the closed conformation of the Mlc1p C-lobe is very similar to that found for calmodulin proteins, suggesting a common opening-closure mechanism for all the myosin light chains. The differences among Mlc1p and other calmodulins are mainly localized in the N-lobe that shows, in the case of Mlc1p, a rather compact and stable structure characterized by some features that are unique to this protein. We show that these features differentiate the interaction mode of CaM and Mlc1p when they interact with the first IQ motif of the class V myosin Myo2p.

EXPERIMENTAL PROCEDURES

Cloning and Plasmid Construction—For pET15b-*CMD1*, a 0.48-kilobase fragment containing *CMD1* was amplified by PCR using the oligos *CMD1*/13/NdeI forward (5′-ATAAAAAAGTCATATGTCCTCCAATCTTACCGAAG-3′) and *CMD1*/+460/BamHI reverse (5′-AATCACAAGGATCCACCTATTTAGATAAC-3′ and genomic K699 DNA as template (16); the fragment was digested with BamHI-NdeI and cloned into the BamHI-NdeI sites of pET15b.

For pET15b-*MLC1*, a 0.48-kilobase fragment containing *MLC1* was amplified by PCR using the oligos *MLC1*/-12/NdeI forward (5′-CATAGAATACATATGTCAGCCACCAGAGCCAATAAAG-3′) and *MLC1*/+471/BamHI reverse 5′-TAAATTTGTGGATCCGCACTCTCATTGTCTC-3′ and as DNA template YCp111*MLC1* (16); the fragment was digested with BamHI-NdeI and cloned into the BamHI-NdeI sites of pET15b.

Protein Expression and IQ Interaction—^{15}N- or ^{13}C,^{15}N-labeled Mlc1p were expressed in *Escherichia coli* cells BL21(DE3) using a pET-15b expression vector. The cells were grown in M9 minimal media containing $(^{15}NH_4)_2SO_4$ and [^{13}C]glucose. Expression was achieved by incubating the cells with 1 mM isopropyl-β-D-thiogalactopyranoside at an A_{600} of 0.7 for 4 h at 37 °C. The protein was purified by affinity chromatography on a nickel nitrilotriacetic acid column (Qiagen). Further purification of the protein was achieved by gel filtration chromatography (prepSuperdex 75, Amersham Biosciences).

Synthetic peptides corresponding to the first three IQ motifs of Myo2p (KMHNSIVMIQKKIRAKYYRKQYL, QISQAIKYLQNNIKGFIIRQRVNDE, and MKVNCATLLQAAYRGHSIRANVF, corresponding to IQ1, IQ2, and IQ3, respectively) were purchased from C4T (Rome, Italy). Aliquots corresponding roughly to 0.2 eq of the IQ peptide were added stepwise to Mlc1p, and the titration was monitored by collecting two-dimensional ^{1}H,^{15}N HSQC spectra after each addition. The peptide was added until no change in the spectrum was detected. The pH was fixed at 6.5, and the Mlc1p concentration was ~0.2–0.4 mM.

NMR Spectroscopy—NMR samples contained 0.8 mM Mlc1p in 60 mM phosphate buffer, pH 6.9, 0.33 M NaCl, and 0.01% NaN_3. All NMR spectra were recorded at 298 K on a Bruker Avance 700 MHz spectrometer equipped with pulsed field gradient triple resonance probes.

Distance restraints were obtained from ^{15}N NOESY-HSQC and aromatic and aliphatic ^{13}C NOESY-HSQC spectra. A set of $^3J_{HNH\alpha}$ was determined by measuring cross-peak intensities in the HNHA spectrum. Residual dipolar couplings (RDCs) were measured using two different salt concentrations. At 0.33 M NaCl, the IPAP experiment (20) and the three-dimensional HACACO (21) were used for the measurements of HN-N and Hα-Cα RDC, respectively. At 0.1 M NaCl, variations of the experiments described by McFeeters *et al.* (22) were used for the HN-N and Cα-CO RDC measurements. These experiments, which are based on the J-modulation of the signal corresponding to the HN, were separated in two-dimensional using the CO nuclei instead of the N nuclei. The three-dimensional HACACO (21) was used for Hα-Cα RDC measurement. The samples used for RDC also contain 16 mg/ml filamentous phage Pf1 (Asla Labs) to induce the molecular alignment. The Mlc1p·IQ1complex was partially assigned by analysis of HNCO, HNCA, CBCAcoNH and HACACO experiments. The NMR data were processed and analyzed on Linux and Silicon Graphics workstations using NMRPipe (23) and NMRView (24) programs.

^{15}N relaxation measurements were conducted at 700 MHz at pH 6.8 and 25 °C temperature. Protein concentration was 1.5 mM. Results are shown in the supplemental data.

Structure Calculation—Structure calculations and refinement were performed with XPLOR-NIH (25). For the N-lobe structure calculation (residues 2–79) we used the refinement protocol described by Chou *et al.* (26) and a set of 93 HN-N, 97 Hα-Cα and 42 Cα-CO RDCs, obtained by combining the two salt concentrations. After the two-step refinement process, a structure representing the free N-lobe was obtained and deposited together with the constraint list in the Protein Data Bank (code 2FCD).

The C-lobe structure (residues 80–149) was calculated using a simulated annealing protocol (27) and a refinement against a data base of Ramachandran plot dihedral angles (28, 29). Backbone dihedral restraints (φ and ψ angles) were derived from chemical shift analysis using the program TALOS (30). A set of 118 ^{1}H,^{15}N, 83 H_α-C_α, and 53 Ca-CO residual dipolar couplings was included in the refinement. Fitting of the observed RDCs to a preliminary structure using the singular value decomposition (SVD) method (31, 32) within the PALES pro-

gram (33) provided an initial guess for the magnitude and orientation of the molecular alignment tensor for each of the two alignment conditions used. Subsequently, these values were optimized during the simulated annealing process The ensemble of the 20 lowest energy target function structures (from a total of 500), in which the number of residues in favored regions of Ramachandran plot is higher than 90%, was chosen to represent the protein solution structure and together with the constraints lists were deposited in the Protein Data Bank (code 2FCE). The programs AQUA and PROCHECK (34) were used to analyze the structures. Table 1 reports the structural statistics. To carry out a complete cross-validation of RDCs, a series of simulated annealing calculations were performed, each lacking 10% of the RDCs (randomly chosen from the whole dataset) (35). The missing RDCs in each run were back-calculated to determine how well each RDC could be predicted; an average R_{free} of 0.25 ± 0.08 was obtained.

RESULTS

When we started this work three structures of uncomplexed proteins in the metal-free form belonging to the calmodulin family were already published. NMR structures were available for *Xenopus laevis* calmodulin, CaM (PDB code 1CFD) (36) and of *S. cerevisiae* calmodulin, Cmd1 (PDB code 1LKJ) (37). The structure of the Mlc1p homologue of *Schizosaccharomyces pombe*, Cdc4p, was also published (PDB code 1GGW) (38) The two calmodulin proteins exhibit very similar conformation of the N and C domain. On the other hand, Cdc4p was described as having a very unusual open conformation for the C-lobe, very different from that of the two calmodulins. This result suggests a significant difference between calmodulin and other myosin light chains that can be interpreted as the basis of a different transition between the free and bound states. In view of that, we have decided to determine the solution structure of uncomplexed Mlc1p, which can be used to test this hypothesis.

The complete assignment of Mlc1p was already described (Biological Magnetic Resonance Bank (BMRB) entry 6332) (39). In this work we have characterized by NMR the solution structure of Mlc1p using a combination of RDCs, ^{1}H-^{1}H distances derived from NOEs, and dihedral information derived from three bonds HN-Hα coupling constants and chemical shift information. RDCs are nowadays used as a complement to more classical NMR-derived constraints like interproton distances and angles (40). The orientation information that is contained in RDCs constitutes valuable information that helps to define more precisely the conformation of a protein in solution. To obtain this information, it is necessary to partially align the protein in a liquid crystal medium. As Mlc1p an acidic protein, the use of Pf1 liquid crystal (41) is particularly advantageous for the measurement of RDCs. In this work we have explored the possibility of having two different degrees of alignment by changing the salt concentration. In fact, the alignment is the consequence of electrostatic repulsion between negative charges located in the filamentous phage and the protein. Low salt concentration will favor a higher degree of alignment, whereas increasing amounts of salt will shield the repulsion, leading to smaller values of the observed RDCs. In this study we have used salt concentrations of 0.33 M and 0.1 M (NaCl). No change in chemical shift was evident between these two experimental conditions, indicating that the structure remains unaltered. A set of 231 and 256 RDCs were measured for the N-lobe and the C-lobe, respectively, combining the two alignment conditions. These include one bond ^{1}H-^{15}N, ^{1}Hα-^{13}Cα (for both salt concentrations), and ^{13}Cα-^{13}C′ couplings (only for the lower salt concentration). In a first analysis, the constants were combined and used to compare the solution structure of the N and C lobes with those of the two crystal structures of Mlc1p complexed with IQ4 (PDB code 1M46) and IQ2 (PDB code 1M45) (10). In 1M46 the N-lobe does not participate in the peptide binding, whereas in 1M45 it contacts the peptide. Fits are performed separately for the N- and C-terminal domains of Mlc1p because, as already observed for CaM and other proteins of this family, the two domains align to different degrees. The results are shown in Fig. 1.

The N-lobe Conformation Does Not Change between Free and Bound Forms of Mlc1—Fitting of the RDCs to the N domain belonging to the crystal structures 1M46 and 1M45 is shown in Figs. 1, *A* and *B*. A good agreement was obtained for 1M46, corresponding to a correlation coefficient of the SVD fit (R_{SVD}) of 0.96 or a quality factor Q (42, 43) of 29% (Fig. 1*A*). A slightly poorer correlation was obtained for the N-lobe of 1M45 (R_{SVD} = 0.94, Q = 35%; Fig. 1*B*), most likely reflecting minor variations occurred upon binding with the peptide. Three conclusions can be drawn from these results. First, the solution structure and the crystal structure of the non-complexed N-lobe are very similar, giving the high sensitivity of the Q factor upon small changes in conformational properties and that a Q factor less than 30% still represents a good agreement between the two structures (43). Second, the good agreement observed for RDCs measured for helices as well as loops anticipates a stable conformation with only moderate flexibility of the loops. Third, although the Q factor is slightly higher for the complexed N-lobe (Fig. 1*B*), conformational variations induced by interaction with the IQ peptide are not significant.

To calculate a solution structure of Mlc1p N-lobe that fits the observed RDCs, we have followed the refinement protocol described by Chou *et al.* (26). As demonstrated for the case of other proteins of the calmodulin family (26), this simple dipolar refinement procedure can be used to examine conformational changes of a protein without going through the time-consuming NOE analysis, especially those belonging to aliphatic side chains. In the present case the result obtained by fitting the observed RDCs to the crystal structure of 1M46 already anticipated only slight variations. The N-lobe exhibits the expected topology with two EF-hand motifs. Four helices are observed, in line with the experimental values of the HN-Hα scalar couplings and chemical shift index analysis (data not shown): helix A (7–14), helix B (24–34), helix C (40–48), and helix D (61–70). Helix A results in solution shorter than the one observed in the 1M46. In the last structure, helix A starts at residue 4. A number of experimental evidences, however, show that this is not the case for the solution structure. Both HN-Hα coupling constants and Cα chemical shifts indicate that residues 4–6 are not in helical conformation. This observation is also sustained by ^{15}N relaxation measurements (see the supplemental data). It is worth noting that in the IQ2 complex (1M45), helix A pre-

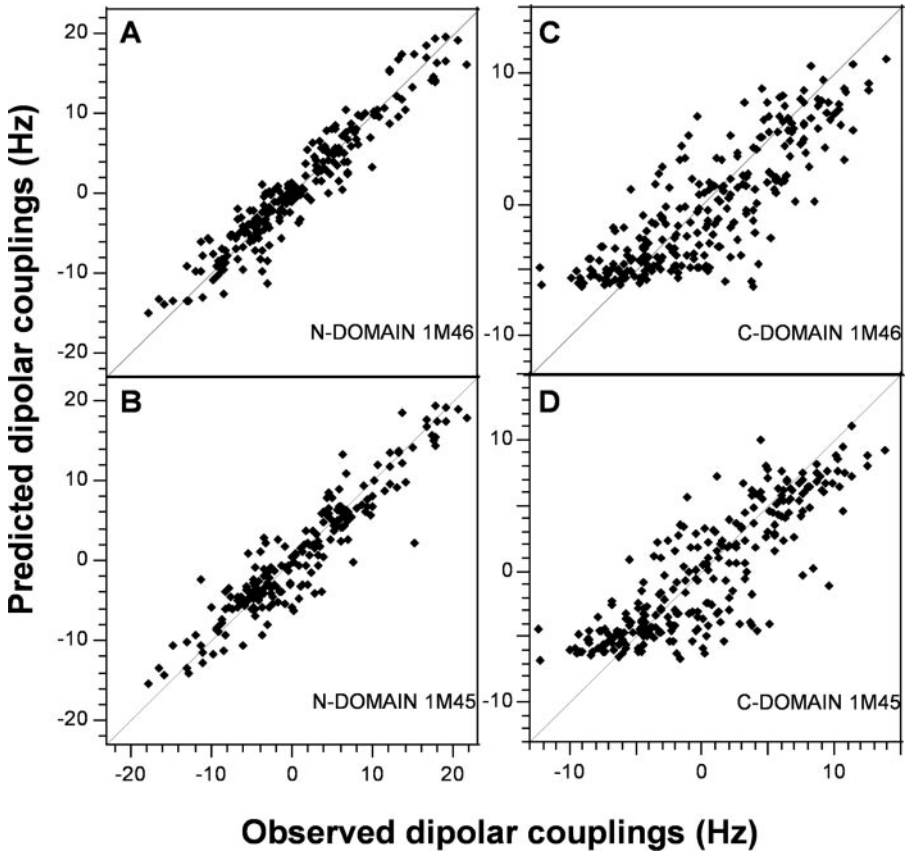

FIGURE 1. **Comparison between normalized observed backbone dipolar couplings measured for uncomplexed Mlc1p and couplings predicted for the x-ray structures of Mlc1p-IQ2 (PDB entry 1M45) and Mlc1p-IQ4 (1M46) complexes using an alignment tensor obtained from the SVD fit.** All dipolar couplings, which include $^1D_{HN}$, $^1D_{H\alpha C\alpha}$, and $^1D_{C\alpha C'}$, are normalized to $^1D_{NH}$ and correspond to the two different alignment conditions used (see "Experimental Procedures"). *A* and *B* show the fitting for the N domain (residues 7–79) against the IQ4 and IQ2 complexes, respectively. *C* and *D* show the corresponding fittings for the C domain (residues 82–148).

sents the same length and involves the same residues to that of free Mlc1p.

An extra portion of helix, helix D′ (72–77), is observed, involving residues that in other calmodulin-like proteins are part of the linker connecting the two lobes (see below). In line with this observation, low values were measured for the HN-Hα coupling constants and clear evidence is also found in the chemical shift index for Cα nuclei (Fig. 2*B*). The kink between helices D and D′ occurs at the level of Asn-71, for which a large HN-Hα coupling constant was measured (9.6 Hz). Further evidence for the stability of this region was obtained through ^{15}N relaxation measurements, indicating that residues 72–77 show ^{15}N T_1 and T_2 and {^{1}H}-^{15}N NOE of similar values to the other four helices in the N-lobe (see the supplemental data).

The backbone r.m.s.d. between helices of the refined N-lobe and that of 1M46 is 0.7 Å. This very low value reflects the similarity of the solution and crystal structures. The NMR refined structure of the N-lobe is also very similar to the conformation observed for 1M45, where the N-lobe is involved in the interaction with the peptide (r.m.s.d. 0.9 Å for the helices backbone). This result corroborates the fact that the interaction with the N-lobe does not affect significantly its conformation.

The Structure of the N-lobe of Mlc1p Presents Unique Conformational Features—The N-lobe of Mlc1p shows very similar spatial disposition for helices A-D as compared with the other three light chains already described in the literature, namely apo-forms of calmodulin and Cdc4p. r.m.s.d. for backbone atoms (r.m.s.d.$_{bb}$) of 1.1, 1.3, and 1.5 Å were obtained for superposition of the four common helices with 1CFD, 1LKJ, and 1GGW, respectively (see Fig. 2 for a superposition with 1CFD). Mlc1p is the only one that presents helix D′ (residues 72–77). Amino acids belonging to helix D′ make a series of contacts that seem to confer extra stabilization to the closed conformation. In fact, in the crystal structures of complexes of Mlc1p with IQ2 and IQ4, the side chain of Leu-75 points directly to the center of the hydrophobic core of the N-lobe, and the side chain of Thr-78 makes a double hydrogen bond contact with Asn-37, belonging to the loop connecting the two EF-hand motifs (Fig. 2*A*). This is particularly relevant because this loop is directly involved in the interaction with IQ2 and IQ3 (10, 18). We have observed a number of interresidue NOEs supporting the Asn-37–Thr-78 interaction in solution as well as the participation of Leu-75 to the hydrophobic core of the protein (Fig. 2*C*). These results show that the solution and crystal structures of the N-lobe are, within experimental error, undistinguishable.

Although Mlc1p presents an extra helix, it displays a clear interdomain flexibility. This is reflected mainly by the fact that the alignment tensor calculated for the two lobes on the basis of the observed RDCs does not coincide. In fact, at low salt concentration the N-lobe showed values of $D_{aNH} = 10.8$ Hz and $R = 0.44$, whereas the C-lobe showed a $D_{aNH} = 6.9$ Hz and $R = 0.53$ using 15 mg ml^{-1} Pf1 liquid crystal. Analysis of chemical shift index as well as ^{15}N T_2 and ^{1}H-{^{15}N} NOEs (data not shown) reveals the existence of flexibility for residues 80–83. These residues show both a larger ^{15}N T_2 (average value 115.5 ± 19.8 ms at 700 MHz) and a lower ^{1}H-{^{15}N} NOE (0.5 ± 0.1) than the average values observed for residues in the helices of Mlc1p N-lobe (89.3 ± 7.4 ms and 0.82 ± 0.1, respectively). The interdomain flexibility of Mlc1p is analogous to that observed for apoCaM (44) and is the consequence of having a linker of similar length. ApoCaM shows a longer helix A (residues 6–19) compared with Mlc1p (residues 7–14). This six-residue difference is compensated in Mlc1p by the presence of the D′ helix (residues 72–77) toward the C terminus of the N-lobe. The disordered linker that connects the two lobes is constituted by 5 amino acids in apoCaM (residues 77–81) and by 4 amino acids in Mlc1p (residues 80–83).

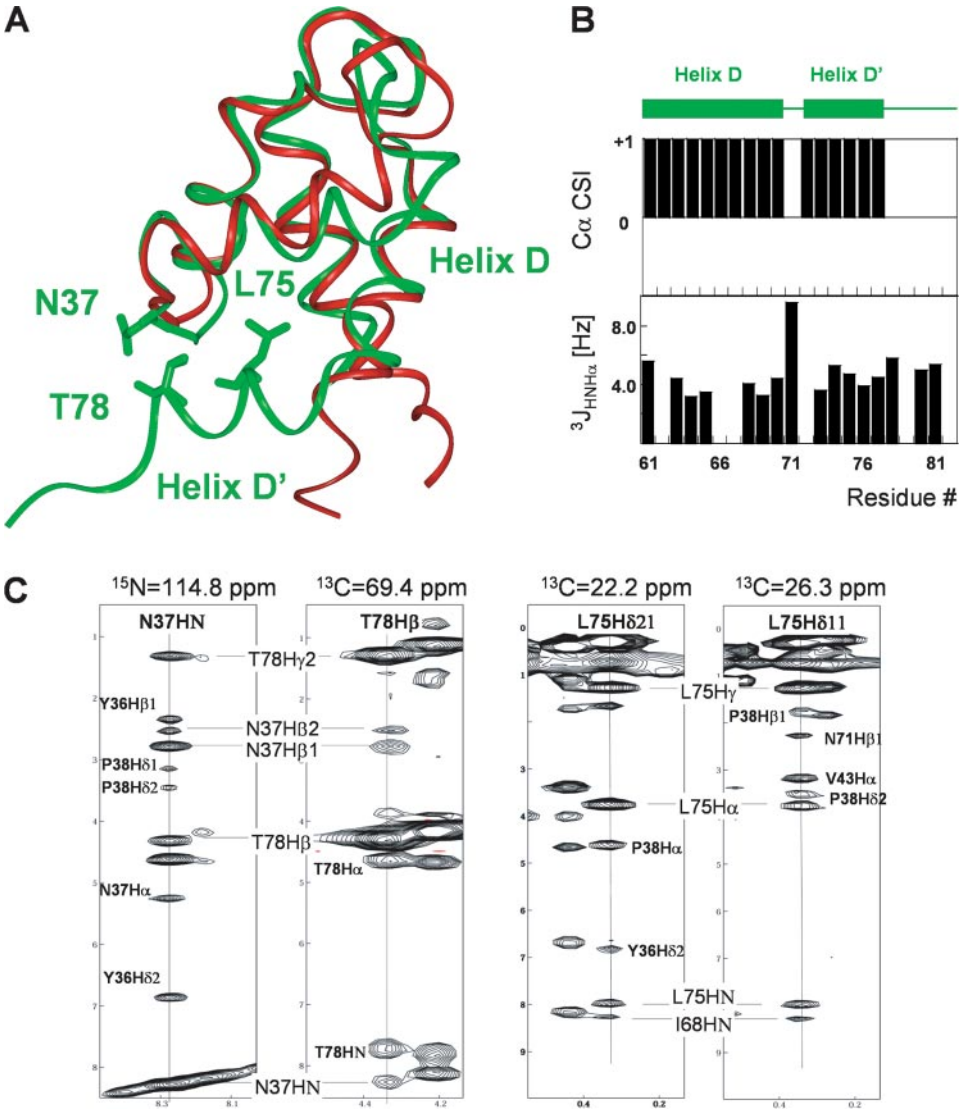

FIGURE 2. **An N-domain structure comparison between Mlc1p (PDB entry 1M46 (10), *green*) and apoCaM (PDB entry 1CFD, *red*).** Structure superposition was performed considering backbone atoms belonging to residues of the four helices: 5–14, 26–32, 40–48, and 61–68 (Mlc1p) and 10–19, 31–37, 45–53, and 65–72 (apoCaM). *Highlighted* are residues that confer special structural features to Mlc1p; Leu-75, that is added to the hydrophobic core of the N-lobe, and Thr-78 and Asn-37, which interact through hydrogen bonds. Asn-37 is a key residue for the regulation of the interaction between the N-lobe and IQ-spanning peptides. *B*, chemical shift index for Cα and $^3J_{HNH\alpha}$ measured for helix D and helix D′. *C*, strips from ^{13}C- and ^{15}N-edited NOESY spectra showing the interaction between Thr-78 and Asn-37 and several NOEs from Leu-75 methyl groups.

have a high affinity for Mlc1p or apoCaM (10, 18). A borderline situation is expected for IQ1, which shows an alanine at position 7 and the consensus arginine at position 11 (Fig. 3*A*) and for which two different hypothesis have been made. In a first analysis it was concluded that even a small side chain like that present in an alanine would display an unfavorable steric hindrance for the Mlc1p N-lobe binding (10). Subsequently, it was observed that apoCaM was able to bind to IQ1 using both lobes by means of a fluorescence resonance energy transfer analysis (18). Although this result was extrapolated to the behavior of Mlc1p, we were interested in testing a possible difference between Mlc1p and CaM in this regard.

To this end increasing amounts of IQ1 peptide were added to a ^{13}C,^{15}N-labeled sample of Mlc1p. Fig. 3*B* shows selected regions of the ^{1}H,^{15}N HSQC spectra obtained after each addition. From these experiments it was evident that peaks belonging to the N-lobe remained unaltered both in chemical shift or line shape, whereas most peaks corresponding to the C-lobe showed a decrease in intensity and almost disappeared after addition of 0.5 eq of the peptide. Beneath this point, new peaks appeared, belonging to the bound form of the protein. Analysis of the peak intensity behavior allowed classification of the exchange regime as slow to intermediate, characterized by an exchange kinetic constant smaller than the difference in chemical shift between the two interconverting states but not sufficiently small to ensure a constant line width during the whole titration.

Mlc1p and CaM Differ in Their Interaction with IQ1—Based on the available structures of complexes between IQ2, IQ3, and IQ4 of Myo2p and Mlc1p, two different binding modes were observed. They differ in the fact that the N-lobe binds (IQ2, IQ3) or not (IQ4) to the peptide. This situation seems to be regulated by a number of factors, and the most important was identified in the presence of a glycine residue in relative position 7 and an arginine in position 11 (see Fig. 3*A*). These residues are present in IQ2 and IQ3 but not in the other four IQ motifs. Analysis of the N-lobe surface shows that there seems not to be enough space to accommodate any residue bearing a side chain in position 7. Based on this assumption, it is clear that IQ4 and IQ6, which show residues different from glycine and arginine at positions 7 and 11, will not allow the N-lobe to bind. A peptide spanning the IQ5 sequence has been shown not to

The absence of progressive peak shifts precludes the transfer of the assignment from the free form to the bound form. For this reason the assignment of the bound form of Mlc1p was done by inspection of HNCO, HNCA, CBCAcoNH, and HACACO experiments in comparison with the known chemical shifts of the free protein. In this way a complete assignment was obtained for the N-lobe, whereas for the C-lobe it was possible to assign 75% of the total HN groups. Fig. 3*C* shows the differences in chemical shifts for the HN group. From this result it can be concluded that the N-lobe of Mlc1p is not involved in the interaction with IQ1. No differences in chemical shift were detected for those regions that contact the peptide in the IQ2 complex (10), namely, residues 10–13 of helix A, 29–34 of helix

A

Consensus		XXXXX	**B**	XX	**BQ**	XX	**BRG**	XX	**BR**	XX	**B**	XXX	
Myo2p	IQ1	^{783}KMHNS	**I**	VM	**IQ**	KK	**IRA**	KY	**YR**	KQ	**Y**	L	^{805}
	IQ2	^{806}QISQA	**I**	KY	**LQ**	NN	**IKG**	FI	**IR**	QR	**V**	NDE	^{830}
	IQ3	^{831}MKVNC	**A**	TL	**LQ**	AA	**YRG**	HS	**IR**	AN	**V**	F	^{853}
	IQ4	^{854}SVLRT	**I**	TN	**LQ**	KK	**IRK**	EL	**KQ**	RQ	**L**	KQE	^{878}
	IQ5	^{879}HEYNA	**A**	VT	**IQ**	SK	**VRT**	FE	**PR**	SR	**F**	L	^{901}
	IQ6	^{902}RTKKD	**T**	VV	**VQ**	SL	**IRR**	RA	**AQ**	RK	**L**	KQ	^{925}

B

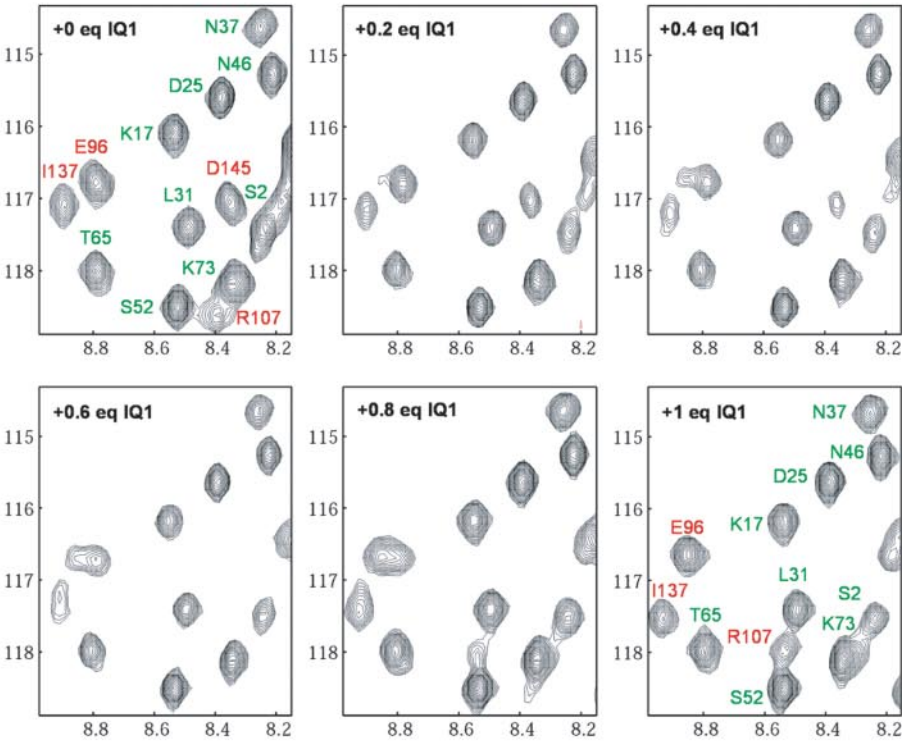

C

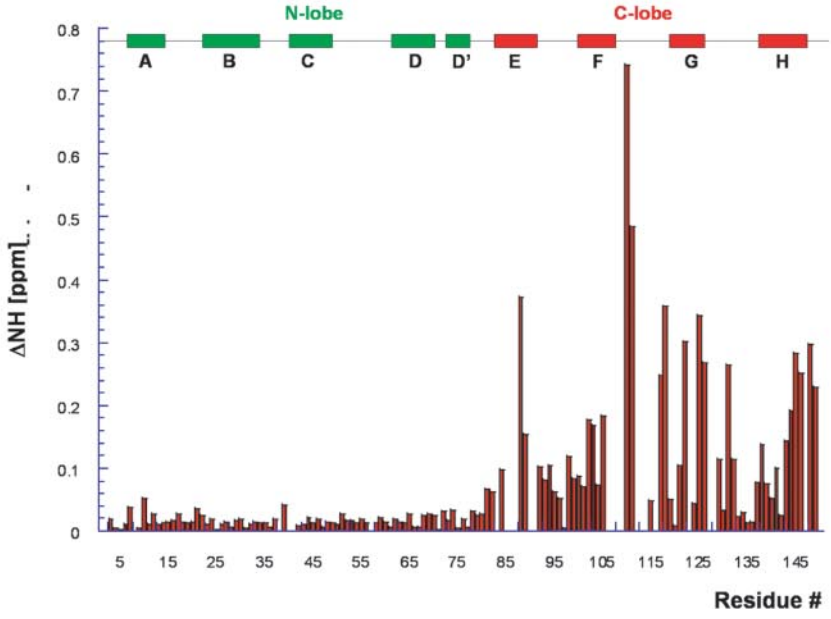

B, and the whole loop 35–38 linking the two EF-hand motifs. Moreover, one of the regions that is expected to exhibit the largest deviation when a compact complex is formed is that of the flexible linker connecting the two lobes, which in the case of Mlc1p is formed by residues 80 to 83. No significant difference was observed for those residues between the free and bound form, indicating that some sort of flexibility still remains in the bound state.

Regarding the affinity constant for the complex formation, we can estimate the magnitude of K_D by evaluation of the exchange kinetics. Because of the line broadening observed, it can be concluded that k_{off} must be 0.1 to 0.05 times the $\Delta\delta$, expressed in Hz. Larger values for k_{off} would cause a more severe line broadening, whereas smaller values would produce non-detectable line broadening during the titration. Considering the observed chemical shift differences for the HN nuclei of some representative peaks of the C-lobe, we can calculate that a k_{off} between 5 and 20 s^{-1} is compatible with the observed line shape behavior. Such a value for k_{off} would be in line with a K_D for the complex in the low nanomolar range if the association process is controlled exclusively by diffusion. This result is consistent with the formation of a relatively stable complex, as suggested by the structure of an analogous bimolecular system such as Mlc1p-IQ4.

As a control experiment we performed titrations on ^{15}N-labeled Mlc1p using peptides spanning both IQ2 and IQ3 binding sites. Fig. 4*A* shows that, different from what was observed in the IQ1 titration, the addition of 1 eq of IQ2 or IQ3 provokes the disappearance of several N-lobe signals, including Asn-37. A complete analysis of signals that were perturbed in the IQ2-IQ3 titrations is depicted in Fig. 4*B*. As can be seen, regions experimenting shifts during the interaction map may very well be those residues that in the crystal structures are directly or indirectly in contact with the peptide. Interestingly, also helix D′ experience shifts during the titration, which is a consequence of its coupling (through Thr-78 and Leu-75) to the Asn-37 loop.

The differential behavior between Mlc1p and CaM for the binding of IQ1 can be explained taking into account the structure of the N-lobe of the two proteins. In the case of peptide binding, the N-lobe exposes a rather flat surface to the helical target. As a consequence, side chains of interacting residues of the peptide are forced to assume an extended conformation. The glycine residue at position 7 was already recognized as a key determinant for the N-lobe binding (10). The impossibility of binding a peptide with another residue in this position comes from the fact that there is a close proximity of the Cα of the glycine and the Asn-37 side chain. The presence of the methyl group of the alanine residue should be accommodated by shifting the loop that is held in this position by the interaction between Asn-37 and Thr-78 (Fig. 5). This interaction and the presence of D′ helix seems to be a unique feature of the N-lobe of Mlc1p and was not detected in any other member of the family. Asn-37 is located in the linker that connects the two EF-hand motifs of the N-lobe. The same region was observed as part of the binding surface between apoCaM and an IQ motif corresponding to the calmodulin-binding domain of neurogranin (45). Calmodulin can adapt itself more easily to make the interaction, possibly by shifting the linker spanning residues 40–44. The absence of helix D′ behind the linker would allow a more versatile adaptation of the linker conformation to different amino acid sequences.

The C-lobe of Mlc1p Undergoes a Major Rearrangement upon Peptide Binding—As Fig. 1, *C* and *D* show, the correlation between observed and calculated RDCs using the C domain of 1M46 and 1M45 as templates is very low. Different from what was already discussed for the N-lobe, high Q values of 0.57 (1M46) and 0.54 (1M45) were observed. This result clearly reflects the transition from the closed to the semi-open states of the C domain. In view of the significant differences expected for the free structure, we have tackled a structure calculation of the C-lobe of Mlc1p using a constraint set including 843 interproton NOEs, dihedral information obtained by combination of HN-Hα coupling constants as well as chemical shift analysis, and a large set of RDCs obtained in the two already described alignment conditions. Table 1 summarizes the most relevant statistical features of the 20 lowest energy structures obtained, and Fig. 6*A* shows the superposition of these 20 structures to their geometrical average. A very good convergence was obtained, reflected by the low value of the r.m.s.d.$_{bb}$ between the structures and their geometrical average.

The structure of the free C-lobe in solution reveals significant differences with respect to the semi-open conformation found in 1M46 and 1M45 (Fig. 6*B*). This lobe presents the four helices involving the same residues observed in the crystal structures: helix E (84–91), helix F (103–109), helix G (119–126), and helix H (139–147). The r.m.s.d.$_{bb}$ between C-lobes of free Mlc1p and those of 1M45 (2.4 Å) and 1M46 (2.3 Å) complexes clearly reflect the opening-closure mechanism that this region undergoes from the free to the bound state. A more clear representation of the differences between these two states of the C domain can be obtained superimposing those regions that remain invariant. These regions could be recognized by inspection of the chemical shift perturbation caused by interaction

FIGURE 3. **Interaction of Mlc1p with a peptide spanning the IQ1 sequence of Myo2p.** *A*, sequence alignment of the six IQ motifs present in Myo2p. The consensus IQ sequence is shown on *top*, where the letter B indicates positions generally occupied by hydrophobic amino acids. Amino acids that interact with the C and N lobes of the light chain in a compact structure like that of the Mlc1p-IQ2 complex are shown in *red* and *blue*, respectively. Amino acids depicted in *green* correspond to mutations compared with the consensus sequence and may be associated with a different conformation of the bound light chain. *B*, titration followed by ^{1}H,^{15}N HSQC experiments of the interaction between Mlc1p and a peptide corresponding to IQ1. In each *panel* the quantity of peptide added is indicated. Also, the assignments of the free and bound Mlc1p for the selected region are indicated for the first and final points of the titration. *Green labels* correspond to amino acids belonging to the N domain, which do not show any significant chemical shift perturbation. As shown in the figures, the HN group of Asn-37, which is expected to interact directly with Ala-797 of IQ1 based on the structure of the IQ2 complex, displays no change in chemical shift between the free and bound states. On the contrary, amino acids indicated in *red* and belonging to the C domain show changes in chemical shifts. *C*, quantification of the HN chemical shift perturbation as a function of residue number. The index, which weights both the chemical shift changes of the ^{1}H and ^{15}N nuclei of the amide group, is obtained by the following equation: $\acute{A}NH = [(\acute{A}\sigma^2_{NH} + \acute{A}\sigma^2_N/25)2]^{1/2}$, where and are the differences in chemical shift between the free and complexed proteins for the H and N, respectively. The secondary structure elements of Mlc1p are also shown on the *top* of the *panel*.

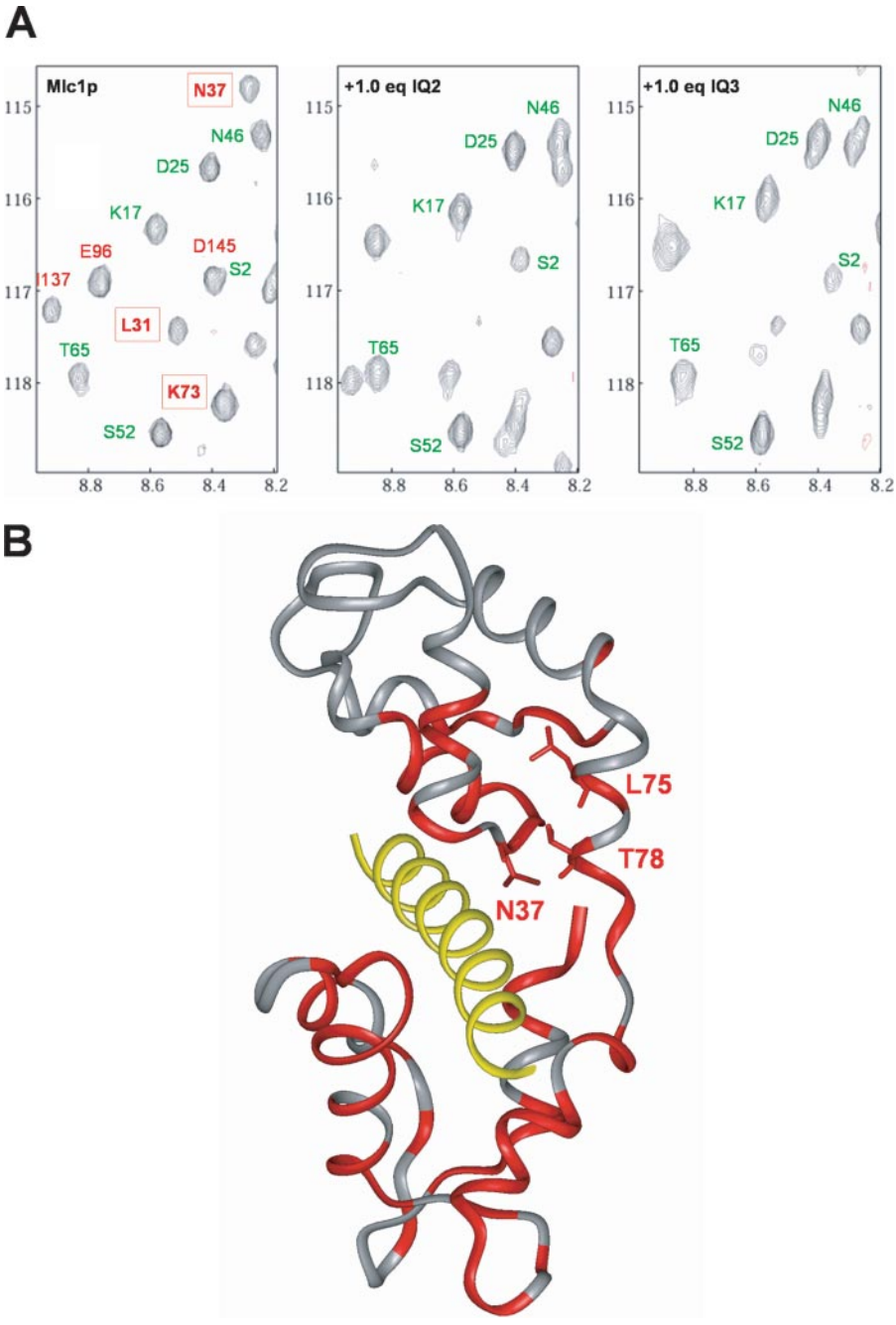

FIGURE 4. **Interaction of Mlc1p with IQ2 and IQ3.** *A*, selected region of the $^{1}H,^{15}N$ HSQC spectra recorded for free Mlc1p and after the addition of 1 eq of IQ2 and IQ3, respectively. Peaks depicted in *green* showed no shift during the titration. In *red* we have indicated the peaks of residues belonging to the C-lobe and in *red* with the *box* those of the N-lobe, which showed perturbation caused by the interaction. *B*, residues showing chemical shift changes by IQ2-IQ3 titration are mapped on the crystal structure of the Mlc1p-IQ2 complex (PDB 1M45) (10).

with IQ1 (Fig. 3*C*). In the case of IQ1 complex formation, helices E and H and the loop connecting the two EF-hands motifs (113–120) showed the highest differences in chemical shifts. This is visualized in Fig. 6*B*, where the structures are superimposed excluding those regions. In this way a r.m.s.d.$_{bb}$ of only 1.3 Å was obtained. Inspection of Fig. 6*B* shows that helix E experiments a significant distortion in the bound state to allow the entry of the IQ peptide. In this respect it is more a bend of the helix axis more than a complete movement of the helix that allows the peptide interaction. There is also a significant movement of the loop connecting the two EF-hand motifs (residues 110–118) that together with the already described distortion of helix E opens a channel that can accommodate the peptide (Fig. 6*C*). Finally, a concerted movement of helix H is also evident, adding more space to the peptide side chains. On the contrary, helices F and G as well as loops E-F and G-H remain in a very similar conformation, confirming the small chemical shifts differences observed for those regions in the IQ1 titration. Helix movements are reflected in the different interhelical angles, which change from 127° and 100° in the free form to 100° and 93° in the semi-open conformation for helices E-F and G-H, respectively.

The C-lobe of Mlc1p Is Similar to That of Apocalmodulin but Significantly Different from That of the Available Structure of Cdc4p—To compare the structure of Mlc1p C-lobe with those of the other three EF-hand proteins, the Dali program was used (46). Table 2 summarizes the results obtained, and Fig. 7 shows the structure superposition. Mlc1p C-lobe highly resembles those of apoCaM and Cmd1, with Z-scores around 9, in line with the high sequence identity of the corresponding C lobes (39 and 40%, respectively). Superposition of Cα atoms belonging to the four helices of these molecules is shown in Figs. 7, *A* and *B*.

Mlc1p and its homologue Cdc4p display an even higher sequence identity of the C-lobe (56%) compared with calmodulin. This observation would suggest also a very similar three-dimensional structure. Surprisingly, the two structures show significant divergences. The Z-score is only 3.2, and both the global and restricted-to-the-helices r.m.s.d. are 3.7 Å. This is the consequence of a very dissimilar disposition of the four helices (Fig. 7*C*). Attempts to fit the observed RDCs of Mlc1p to the structure of Cdc4p yielded a very bad correlation even when considering only residues belonging to the helices (R_{SVD} = 0.56, r.m.s.d. = 7.29 Hz). In contrast, the same fitting performed on apoCaM or Cmd1 C lobes yielded a much better agreement (R_{SVD} = 0.93 and 0.92, r.m.s.d. = 3.33, and 3.54 Hz). This is particularly relevant because RDCs are very sensitive to different orientations of the helices and confirm the close analogy

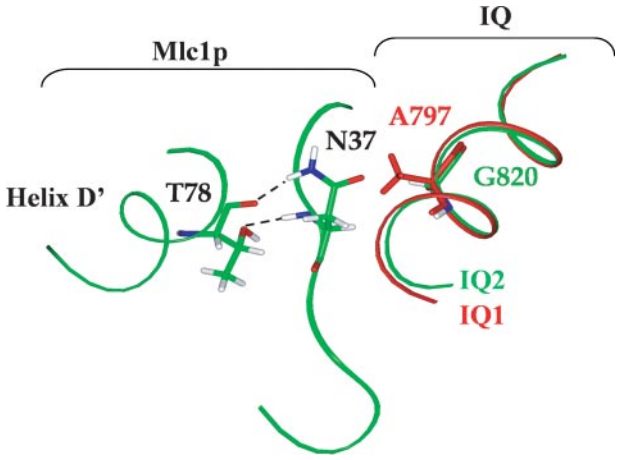

FIGURE 5. **The influence of helix D′ in the binding properties of Mlc1p N-lobe.** The *green* structure corresponds to the crystal structure of the Mlc1p-IQ2 complex (PDB 1M45) (10), showing the close proximity of Asn-37 to Gly-820 and leaving no space for a side chain. In *red* we have modeled the expected conformation of bound IQ1. Ala-797, which now would occupy the position close to Asn-37, would need to cause a shift of the loop. This shift is unlikely to occur because of the extra rigidity imposed by helix D′. On the contrary, calmodulin does not show any D′-helical tract, and consequently, the corresponding loop can shift allowing the interaction between the N domain and IQ1, explaining the compact structure observed by fluorescence resonance energy transfer experiments (18).

of the C-lobe structure of Mlc1p and the two calmodulin structures.

DISCUSSION

Although sharing a high sequence homology with other members of the calmodulin family, Mlc1p N-lobe domain presents some unique structural features. The most striking is the presence of a fifth helix (D′), which seems to confer an enhance stability to the whole closed structure of the N-lobe by providing an extra residue (Leu-75) to the hydrophobic core of the domain. In addition, it plays a central role in holding the conformation of the region directly involved in IQ binding, comprising residues 35–39. Through double hydrogen-bonding, Thr-78 interacts with Asn-37, responsible for binding discrimination favoring only IQ motifs that present a glycine at position 7. This feature is not shared by CaM. As a consequence, binding to IQ1, which presents an alanine in position 7, occurs differently between the two proteins; CaM uses both lobes in this interaction (18), whereas Mlc1p only binds IQ1 through its C-lobe.

Although Mlc1p and Cdc4p exert a similar function, the presence of the D′-helix was not observed in the Cdc4p structure (38). The key residue Leu-75 is replaced by an asparagine, and two acidic residues of Mlc1p (Glu-74 and Asp-76), which are part of the D′-helix are replaced by residues with much less propensity of being in a helix (Pro-68 and Gly-70). Nevertheless, it was noted that a partial folding of this region is induced when the C-lobe is isolated from the N-lobe (47). Thus the D′ helix of Mlc1p is a characteristic belonging only to the structure of Mlc1p and not to other closely related proteins of this family.

The compact structure of the N-lobe Mlc1p as well as the differences noted in the way Mlc1p interacts with IQ1 of Myo2 compared with Cmd1 could explain the differences in the viability and phenotypes of *mlc1* and *cmd1* mutants having alanine substitution in conserved phenylalanine residues located in the

TABLE 1

Experimental restraints and structural statistics for the 20 lowest energy structures of the C-domain of Mlc1p

Number of experimental restraints	1245
Distance restraints from NOEs	843
Intraresidue	274
Interesidue	569
Hydrogen bond distance restraints[a]	23
Dihedral angle restraints	125
ϕ constraints	63
ψ constraints	62
H-N RDCs	118[b]
H_α-C_α RDCs	83[b]
C_α-CO RDCs	53
Average number of restraints per residue	17.8
XPLOR energies (kcal/mol)[c]	
E_{total}	786.0 ± 9.7
E_{bond}	9.3 ± 0.5
E_{angle}	125.0 ± 2.9
$E_{improper}$	29.5 ± 0.8
E_{vdw}	31.2 ± 1.4
E_{cdih}	10.3 ± 0.9
E_{rama}	259.0 ± 4.0
E_{noe}	24.1 ± 6.1
E_{sani}	297.6 ± 3.8
r.m.s.d. from experimental restraints	
Average distance restraints violation (Å)	0.036 ± 0.004
Average dihedral angle restraints violation (deg)	1.13 ± 0.05
Average H-N RDCs violation (Hz)	0.974 ± 0.008
Average H_α-C_α RDCs violation (Hz)	0.667 ± 0.009[d]
Average C_α-CO RDCs violation (Hz)	2.82 ± 0.04[d]
R_{free} %	25 ± 8
r.m.s.d. from idealized covalent geometry	
Bond (Å)	0.00288 ± 0.00007
Angle (°)	0.633 ± 0.007
Improper (°)	0.591 ± 0.008
Ramachandran analysis	
Residues in favored regions (%)	91.5 ± 1.3
Residues in additional allowed regions (%)	6.9 ± 1.3
Residues in generously allowed regions (%)	1.6 ± 0.0
Residues in disallowed regions (%)	0.0 ± 0.0
Coordinates precision	
Backbone (Å)	0.33 ± 0.05
All heavy atoms (Å)	0.90 ± 0.05

[a] HN-O and N-O distances were constrained to 2.1 ± 0.5 and 3.0 ± 0.5 Å, respectively.
[b] Total number for the two alignment conditions used (see text).
[c] vdw, cdih, rama and sani energy terms refer to Van der Waals, dihedral angles, Ramachandran potential and dipolar couplings constraints, respectively.
[d] Normalized to the H-N value.

N-lobe (16, 48). The *mlc1*^{F11A,F14A} allele obtained by site-directed mutagenesis causes lethality when expressed from a low copy plasmid in *mlc1*Δ cells (16, 49). Expression of a similar calmodulin allele, the *cmd1*^{F16A,F19A} *allele*, does not cause lethality, although it causes this protein to mislocalize (48). Similarly to *mlc1*^{F11A,F14A} mutant, the *SpCdc4*^{F12} mutant has a temperature-sensitive phenotype (38). This indicates that Cdc4p and Mlc1p, but not Cmd1, require the conserved phenylalanine residues located within the N-lobe to carry their essential function(s) in the cell. Interestingly it has been observed that mutation within the conserved phenylalanine located in the N lobe or C-lobe of Cmd1 causes defects in their binding with some but not all of their targets (48, 50–53). Thus, the structure differences observed among Cdc4p, Mlc1p, and Cmd1 N-lobe conformation is likely to be one of the factors guiding their target binding discrimination.

Both Cdc4p and Mlc1p share the ability to bind to proteins implicated in vesicle transport and cytokinesis, among which are class II and class V myosin and IQGAP-like proteins (53–55). It was suggested that when Mlc1p binds to Myo2p IQ motifs using

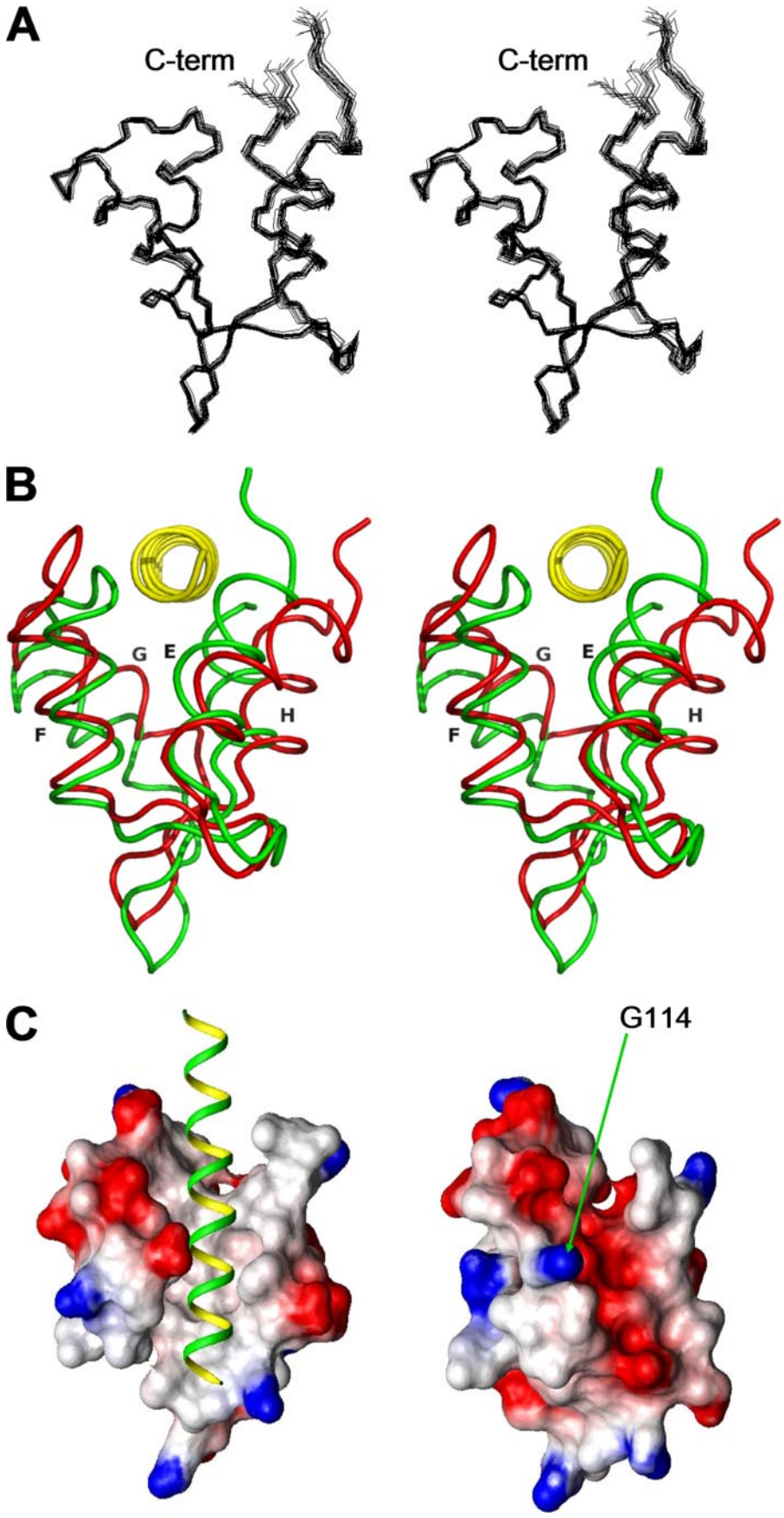

only the C-lobe (IQ4, IQ6, and as demonstrated here IQ1), it may use the N-lobe to contact a second target (10, 16). The ability to bridge to different IQ-like targets using the N-lobe could be particularly important during cytokinesis when Mlc1p, by binding to the class II myosin Myo1p, the IQGAP-like protein Iqg1/Cyk1, and Myo2p, coordinates the events leading to secretory vesicle delivery at septum with those leading to actomyosin ring contraction (15, 16, 55). Indeed, the possibility for the N-lobe of interacting independently from the C-lobe with a sufficient selectivity and affinity has to be demonstrated. It is particularly puzzling how the N-lobe could discriminate among targets because the contact surface between the N-lobe and the IQ motifs is particularly flat and featureless. An obvious possibility to overcome this point is to allow the N-lobe of Mlc1p to adopt a more open conformation. Two signals are known to provoke the opening of a lobe in the calmodulin superfamily, binding to divalent cations or phosphorylation. As was already discussed, Mlc1p cannot bind Ca^{2+}, and so phosphorylation is a plausible alternative (38). For Cdc4p, phosphorylation of Ser-2 and -6 was observed *in vivo*, but their role for Cdc4 function was later on excluded because mutations in these sites do not alter Cdc4p activity or binding abilities (56).

It has been shown recently that GTP can act as a stimulus for Mlc1p and Myo2p interaction. GTP binding to the Rab/Ypt protein Ypt32p, which acts at late stages of vesicle transport, increases Mlc1p binding to Myo2p via the IQ motifs (17). Given the known role of Mlc1p in regulating vesicle-Myo2p interaction during cytokinesis (16), an intriguing possibility is that the differential ability of CaM and Mlc1p to bind to Myo2p IQ1 might play a role in regulating vesicle-motor interaction in response to Rab/Ypt GTP binding.

The Mlc1p C-lobe undergoes a significant rearrangement from the free to the bound state. The relative adjacent position in the free state of helix E and the loop connecting the two EF hands promotes the formation of a negatively charged region that can be important for the electrostatic recognition of IQ motifs (see Fig. 6*C*). Interestingly, mutation of Gly-114, located in this loop, by a negative charge (G114D) was shown to produce cells temperature-sensitive for growth and showed a severe defect in cytokinesis even at 24 °C (57). Mutation of Gly-114 by a Asp would place an extra charge in this region, and this can be a source of destabilization for the closed conformation. In the orthologue Cdc4p a more conservative mutation was observed as leading to a temperature-sensitive phenotype regarding the cellular growth. In this case mutation of the cor-

TABLE 2
Structural homology of the Mlc1p C domain with other calcium-free EF-hand proteins

Protein	PDB	r.m.s.d.[a]	r.m.s.d. helices[b]	Z[c]	No. of residues aligned[d]	% Identity
CaM	1CFD	2.1	1.5	9.1	69	39
Cmd1	1LKJ	2.0	1.3	9.0	68	40
Cdc4p	1GGW	3.7	3.7	3.2	62	56

[a] Positional r.m.s.d. of superimposed Cα atoms in Å, computed by Dali (Holm and Sander (46)).
[b] Calculated for Cα atoms belonging to the four helices only.
[c] Z score computed by Dali. A measure of structural similarity in S.D. greater than that expected. A score of <2.0 indicates two proteins are structurally dissimilar (46).
[d] Number of residues used by Dali in the calculation of the global r.m.s.d. of the third column.

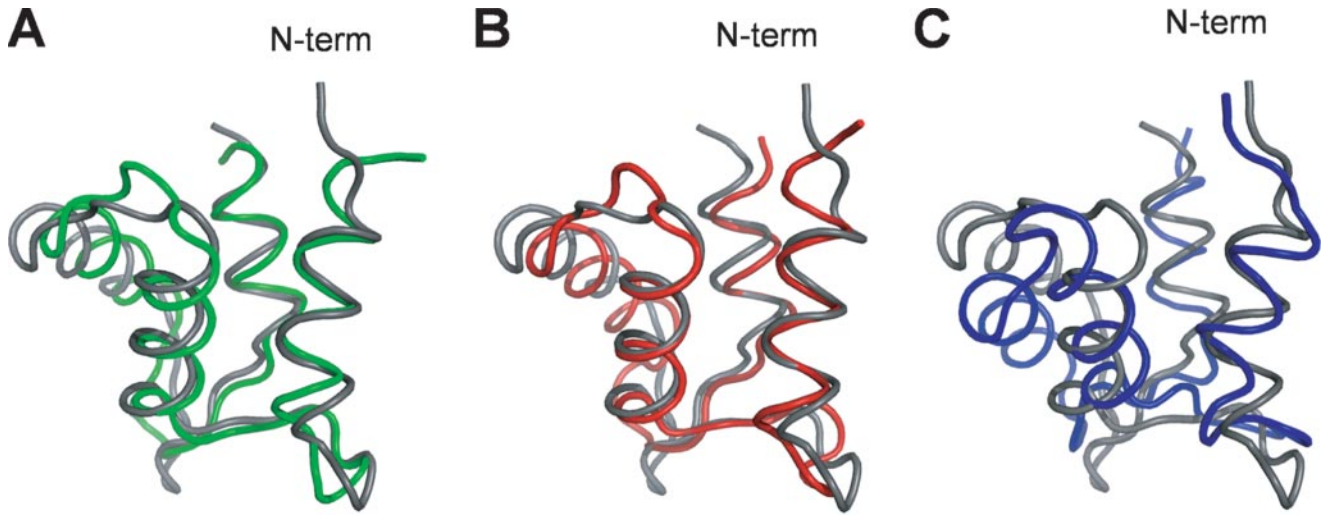

FIGURE 7. **Superposition of the C domains belonging to different light chains.** Mlc1p C domain is shown in the three figures in *green*. *A*, *B*, and *C* show the superposition with apoCaM (1CFD), Cmd1 (1LKJ) and Cdc4p (1GGW), respectively. Residues used for the superposition were 83–112, 135–146 (Mlc1p), 82–111, 134–145 (apoCaM), 82–111, 133–144 (Cmd1), and 76–105, 126–137 (Cdc4p).

FIGURE 6. **Structure of the C domain of Mlc1p.** *A*, superposition of the 20 structures showing lowest energy for the C domain of Mlc1p (residues 82–149). The relative backbone r.m.s.d. relative to the mean is 0.33 Å. *B*, stereoview of the superposition of the average structure for the C-lobe of free Mlc1p (*green*) with the IQ4 complex (*red* for the protein and *yellow* for the IQ4 peptide; PDB entry 1M46). Residues used for the backbone superposition are those showing the highest similarities between the two structures and those for which relatively low chemical shift perturbation was observed in the IQ1 titration. They correspond to residues 96–109 and 118–135. *Letters* indicate the helices of the C-lobe. *C*, electrostatic properties of the surface displayed by the IQ4 complex (*left*) and free Mlc1p (*right*). The IQ4 peptide is shown in *green* and *yellow*. Partial charge are depicted in *red* (negative) and *blue* (positive). Potentials were calculated using MolMol (60). As shown in this comparison, shifts of helices E, G, and H as well as the loop connecting the two EF-hand motifs open a channel for peptide insertion. A large negative region is formed in the free form, which may be used for the protein to direct the right orientation of the positively charged target during the recognition process. Gly-114 belongs to this region, and its mutation by a negatively charged amino acid was already shown to be lethal for the yeast (57).

responding Gly-107 by Ser was observed to give perturbation in the chemical shift of the entire loop (38).

In addition, this loop connecting the two EF-hands could be involved in an intermolecular contact with a second Mlc1p molecule if Mlc1p acts both as RLC and ELC. This model was already proposed for Cdc4p based on a series of observations (38). However, more recent data suggest that the RLC-ELC model cannot be easily adapted to Mlc1p-Myo2p (18). The model suggested for Cdc4p implies binding of Mlc1p to a given IQ in the ELC conformation and in the subsequent IQ as RLC. The only two consecutives IQ motifs to accomplish this seem to be IQ3 (binding as ELC) and IQ4 (binding as RLC). IQ4, however, does not present the amino-acidic sequence characteristic of an incomplete IQ, which is an absolute requirement for the RLC binding mode (19). An alternative model would propose the binding of both Mlc1p and Cmd1. Binding of Ca^{2+} can then promote a different situation in which IQ3 and IQ4 can interact simultaneously with Cmd1, as suggested by data obtained for the interaction of CaM with the murine dilute myosin V (58). This rearrangement would displace Mlc1p from Myo2p IQ3 and would cause a major conformational twist to the "lever arm" of the myosin.

Finally, by comparing both the sequence similarity and structural features of the N- and C-lobes belonging to different light chains, we can draw some general conclusions. Among calmodulin-like proteins with known structure, the C-lobe is more conserved both in length and three-dimensional disposition of the different helices. This lobe carries out most of the interactions that take place during binding of the light chain to the myosin heavy chain that are among the most evolutionary conserved target of these proteins (59). On the other hand, the amino acid composition, loop length, and even the presence of extra helical tracts, as the D′ helix of Mlc1p, seem to confer particular properties to each N-lobe that might specify for their different action in the cells in response to different intracellular signals. We have shown that differences in the structure of the N-lobe confer diverse capabilities to Mlc1p compared with CaM for the interaction with the first IQ motif of Myo2p. These data might explain the different binding abilities of Cmd1 and Mlc1p for Myo2p fragments containing IQ motifs (15)[4] or with IQGAP-like protein Iqg1/Cyk1 (15, 55). The importance of the differences observed in CaM and Mlc1p interaction with Myo2p IQ1 motif are of general interest as Mlc1p has an essential function for correct vesicle targeting to specific location that is not shared by calmodulin. Myosin V-mediated intracellular transport is essential for basic cellular processes, among which are skin pigmentation, immunological and neurological response, cell proliferation, and cytokinesis, and several human dysfunctions have been identified based on defects in myosin V function (13, 61–63). Thus, the ability of a specific light chain to differently regulate myosin V transport capabilities in response to different stimuli could be use in the future as a tool for specific drug intervention.

Acknowledgments—We are deeply indebted to Dr. Wolfgang Wagner for construction of the Mlc1p plasmid used in this study and phenotype analysis of mlc1 mutants and to Dr. Pamela Bielli and Prof. G. Rotilio for helpful discussions.

REFERENCES

1. Sellers, J. R., and Veigel, C. (2006) *Curr. Opin. Cell Biol.* **18,** 68–73
2. Weisman, L. S. (2006) *Nat. Rev. Mol. Cell Biol.* **7,** 243–252
3. May, K. M., Win, T. Z., and Hyams J. S. (1998) *Cell Motil. Cytoskeleton* **39,** 195–200
4. Bahler, M., and Rhoads, A. (2002) *FEBS Lett.* **513,** 107–113
5. O'Day, D. H., and Myre, M. A. (2004) *Biochem. Biophys. Res. Commun.* **320,** 1051–1054
6. Cheney, R. E., O'Shea, M. K., Heuser, J. E., Coelho, M. V., Wolenski, J. S., Espreafico, E. M., Forscher, P., Larson, R. E., and Mooseker, M. S. (1993) *Cell* **75,** 9–11
7. De La Cruz, E. M., Wells, A. L., Rosenfeld, S. S., Ostap, E. M., and Sweeney, H. L. (1999) *Proc. Natl. Acad. Sci. U. S. A.* **96,** 13726–13731
8. Wang, F., Chen, L., Arcucci, O., Harvey, E. V., Bowers, B., Xu, Y., Hammer, J. A., III, and Sellers, J. R. (2000) *J. Biol. Chem.* **275,** 4329–4335
9. Cyert, M. S. (2001) *Annu. Rev. Genet.* **35,** 647–672
10. Terrak, M., Wu, G., Stafford, W. F., Lu, R. C., and Dominguez, R. (2003) *EMBO J.* **22,** 362–371
11. Vetter, S. W., and Leclerc, E. (2003) *Eur. J. Biochem.* **270,** 404–414
12. Li, X. D., Mabuchi, K., Ikebe, R., and Ikebe, M. (2004) *Biochem. Biophys. Res. Commun.* **315,** 538–545
13. Krementsov, D. N., Krementsova, E. B., and Trybus, K. M. (2004) *J. Cell Biol.* **164,** 877–886
14. Wang, F., Thirumurugan, K., Stafford, W. F., Hammer, J. A., III, Knight, P. J., and Sellers, J. R. (2004) *J. Biol. Chem.* **279,** 2333–2336
15. Stevens, R. C., and Davis, T. N. (1998) *J. Cell Biol.* **142,** 711–722
16. Wagner, W., Bielli, P., Wacha, S., and Ragnini-Wilson, A. (2002) *EMBO J.* **21,** 6397–6408
17. Bielli, P., Casavola, E. C., Biroccio, A., Urbani, A., and Ragnini-Wilson, A. (2006) *Mol. Microbiol.* **59,** 1576–1590
18. Terrak, M., Rebowski, G., Lu, R. C., Grabarek, Z., and Dominguez, R. (2005) *Proc. Natl. Acad. Sci. U. S. A.* **102,** 12718–12723
19. Houdusse, A., and Cohen, C. (1995) *Proc. Natl. Acad. Sci. U. S. A.* **92,** 10644–10647
20. Ottinger, M., Delaglio, F., and Bax, A. (1998) *J. Magn. Reson.* **131,** 373–378
21. Cicero, D. O., Contessa, G. M., Paci, M., and Bazzo, R. (2006) *J. Magn. Reson.* **180,** 222–228
22. McFeeters, R. L., Fowler, C. A., Gaponenko, V. V., and Byrd, R. A. (2005) *J. Biomol. NMR* **31,** 35–47
23. Delaglio, F., Grzesiek, S., Vuister, G. W., Zhu, G., Pfeifer, J., and Bax, A. (1995) *J. Biomol. NMR* **6,** 277–293
24. Johnson, B. A., and Blevins, R. A. (1994) *J. Biomol. NMR* **4,** 603–661
25. Schwieters, C. D., Kuszewski, J. J., Tjandra, N., and Clore, G. M (2003) *J. Magn. Res.* **160,** 66–74
26. Chou, J. J., Shipeng, L., and Bax, A. (2000) *J. Biomol. NMR* **18,** 217–227
27. O'Donoghue, S. I., King, G. F., and Nilges, M. (1996) *J. Biomol. NMR* **8,** 193–206
28. Clore, G. M., Gronenborn, A. M., and Tjandra, N. (1998) *J. Magn. Reson.* **131,** 159–162
29. Tjandra, N., Omichinski, J. G., Gronenborn, A. M., Clore, G. M., and Bax, A. (1997) *Nat. Struct. Biol.* **4,** 728–732
30. Cornilescu, G., Delaglio, F., and Bax, A. (1999) *J. Biomol. NMR* **13,** 289–302
31. Losonczi, J. A., Andrec, M., Fischer, M. W., and Prestegard, J. H. (1999) *J. Magn. Reson.* **138,** 334–342
32. Fischer, M. W., Losonczi, J. A., Weaver, J. L., and Prestegard, J. H. (1999) *Biochemistry* **38,** 9013–9022
33. Zweckstetter, M., and Bax, A. (2000) *J. Am. Chem. Soc.* **122,** 3791–3792

[4] E. Caroli Casavola, P. Bielli, A. Catucci, M. Pennestri, D. O. Cicero, and A. Ragnini-Wilson, manuscript in preparation.

34. Laskowsky, R. A., Rullmann, J. A. C., MacArthur, M. W., Kaptein, R., and Thornton, J. M. (1996) *J. Biomol. NMR* **8,** 477–486
35. Clore, G. M., and Garrett, D. S. (1999) *J. Am. Chem. Soc.* **121,** 9008–9012
36. Kuboniwa, H., Tjandra, N., Grzesiek, S., Ren, H., Klee, C. B., and Bax, A. (1995) *Nat. Struct. Biol.* **2,** 768–776
37. Ishida, H., Nakashima, K., Kumaki, Y., Nakata, M., Hikichi, K., and Yazawa, M. (2002) *Biochemistry* **41,** 15536–15542
38. Slupsky, C. M., Desautels, M., Huebert, T., Zhao, R., Hemmingsen, S. M., and McIntosh, L. P. (2001) *J. Biol. Chem.* **276,** 5943–5951
39. Melino, S., Pennestri, M., Santoprete, A., Bielli, P., Paci, M., Ragnini-Wilson, A., and Cicero, D. O. (2005) *J. Biomol. NMR* **31,** 367–378
40. Grishaev, A., and Bax, A. (2005) *Curr. Opin. Struct. Biol.* **15,** 563–570
41. Hansen, M. R., Mueller, L., and Pardi, A. (1998) *Nat. Struct. Biol.* **5,** 1065–1074
42. Cornilescu, G., Marquardt, J. L., Ottiger, M., and Bax, A. (1998) *J. Am. Chem. Soc.* **120,** 6836–6837
43. Ottiger, M., and Bax, A. (1999) *J. Biomol. NMR* **13,** 187–191
44. Tjandra, N., Kuboniwa, H., Ren, H., and Bax, A. (1995) *Eur. J. Biochem.* **230,** 1014–1024
45. Cui, Y., Wen, J., Sze, K. H., Man, D., Lin, D., Liu, M., and Zhu, G. (2003) *Anal. Biochem.* **315,** 175–182
46. Holm, L., and Sander, C. (1993) *J. Mol. Biol.* **233,** 123–138
47. Escobar-Cabrera, E., Venkatesan, M., Desautels, M., Hemmingsen, S. M., and McIntosh, L. P. (2005) *Biochemistry* **44,** 12136–12148
48. Ohya, Y., and Botstein, D. (1994) *Genetics* **138,** 1041–1054
49. Wagner W. (2002) *The Regulation of Vesicle Transport by Rab/Ypt Proteins in Saccharomyces cerevisiae*, University of Vienna
50. Geli, M. I., and Riezman, H. (1996) *Science* **272,** 533–535
51. Geli, M. I., Wesp, A., and Riezman, H. (1998) *EMBO J.* **17,** 635–647
52. Okano, H., Cyert, M. S., and Ohya, Y. (1998) *J. Biol. Chem.* **273,** 26375–26382
53. Desautels, M., Den Haese, J. P., Slupsky, C. M., McIntosh, L. P., and Hemmingsen, S. M. (2001) *J. Biol. Chem.* **276,** 5932–5942
54. D'souza, V. M., Naqvi, N. I., Wang, H., and Balasubramanian, M. K. (2001) *Cell Struct. Funct.* **26,** 555–565
55. Shannon, K. B., and Li, R. (2000) *Curr. Biol.* **10,** 727–730
56. McCollum, D., Feoktistova, A., and Gould, K. L. (1999) *J. Biol. Chem.* **274,** 17691–17695
57. Luo, J., Vallen, E. A., Dravis, C., Tcheperegine, S. E., Drees, B., and Bi, E. (2004) *J. Cell Biol.* **6,** 843–855
58. Martin, S. R., and Bayley, P. M. (2002) *Protein Sci.* **11,** 2909–2923
59. Pashkova, N., Jin, Y., Ramaswamy, S., and Weisman, L. S. (2006) *EMBO J.* **25,** 693–700
60. Koradi, R., Billeter, M., and Wüthrich, K. (1996) *J. Mol. Graph.* **14,** 51–55
61. Rao, M. V., Engle, L. J., Mohan, P. S., Yuan, A., Qiu, D., Cataldo, A., Hassinger, L., Jacobsen, S., Lee, V. M., Andreadis, A., Julien, J. P., Bridgman, P. C., and Nixon, R. A. (2002) *J. Cell Biol.* **159,** 279–290
62. Rudolf, R. Kogel, T., Kuznetsov, S. A., Salm, T., Schlicker, O., Hellwig, A., Hammer J. A., III, and Gerdes, H. H. (2003) *J. Cell Sci.* **116,** 1339–1348
63. Seabra, M. C., Mules, E. H., and Hume, A. N. (2002) *Trends Mol. Med.* **8,** 23–30

Structural Basis for the Interaction of the Myosin Light Chain Mlc1p with the Myosin V Myo2p IQ Motifs

Matteo Pennestri, Sonia Melino, Gian Marco Contessa, Elena Caroli Casavola, Maurizio Paci, Antonella Ragnini-Wilson and Daniel O. Cicero

J. Biol. Chem. 2007, 282:667-679.
doi: 10.1074/jbc.M607016200 originally published online October 29, 2006
